

Self-assembly of amphiphilic peanut-shaped nanoparticles

Stephen Whitelam*¹ and Stefan A.F. Bon²

¹*Molecular Foundry, Lawrence Berkeley National Laboratory,
1 Cyclotron Road, Berkeley, CA 94720, USA*

²*Department of Chemistry, University of Warwick,
Coventry, CV4 7AL, United Kingdom*

We use computer simulation to investigate the self-assembly of Janus-like amphiphilic peanut-shaped nanoparticles, finding phases of clusters, bilayers and micelles in accord with ideas of packing familiar from the study of molecular surfactants. However, packing arguments do not explain the hierarchical self-assembly dynamics that we observe, nor the coexistence of bilayers and hollow, faceted capsids. This coexistence suggests that experimental realizations of our model can achieve multi-potent assembly of either of two competing ordered structures.

Components are said to ‘self-assemble’ when they organize to form stable patterns or aggregates without external direction. Self-assembly is driven by interactions as different as weak covalent bonds and capillary forces, involves components ranging in size from Ångströms to centimeters, and occurs both in inorganic settings and in living organisms [1, 2, 3, 4, 5, 6, 7, 8, 9]. Mimicry of the self-assembly seen in the natural world promises the development of new, functional materials patterned on the nanometer scale [10, 11]. In pursuit of this goal, we take inspiration from the self-assembly of molecular surfactants to investigate using computer simulation the behavior of a simple model of their colloidal counterparts. Molecular surfactants, comprising chemically linked hydrophobic and hydrophilic groups, are of central importance in biology and industry, able to form a plethora of phases in water or mixtures of water and oily liquids. These phases include micelles [12], bilayers and vesicles, as well as numerous bicontinuous phases [13] that serve as internal cellular packaging [14] and are the bane of many a plumber.

Here we ask *What might self-assemble in aqueous solution from amphiphilic, peanut-shaped colloidal nanoparticles?* Such particles can now be prepared in large quantities, starting from spherical, crosslinked polystyrene ‘seed’ particles of radius ~ 50 nm. Mixing these seeds with styrene initiates monomer-polymer phase separation and creates particles with a peanut-like shape characterized by two fused spherical lobes of controllable relative size. Additional treatment of the seed particle renders the resulting peanuts amphiphilic, with one lobe hydrophobic and the other hydrophilic [15, 16, 17]; the resulting amphiphile can be regarded as a generalized Janus particle [18]. (We note that colloidal silica dumbbells can be synthesized by other routes [19], and that micrometer-scale peanuts

* swhitelam@lbl.gov

show potential as Pickering stabilizers of oil-in-water emulsions [20].) In an attempt to answer our posed question we have constructed a model of interacting peanuts whose minimal character is motivated by the insight into self-assembly afforded by similarly simple model systems [21, 22, 23, 24, 25, 26, 27, 28, 29, 30, 31, 32, 33]. Our model can be evolved with computational efficiency sufficient to allow observation of collective, thermally-driven dynamics on timescales of seconds. Its construction rests upon two assumptions: first, that peanuts in aqueous solution experience a thermodynamic driving force that cause hydrophobic lobes to attract each other; and second, that functionalization of peanuts' hydrophilic lobes renders them chemically passive. We assume solution conditions to be such that electrostatic interactions between peanuts mediate only short-ranged repulsions.

Model geometry is shown in Figure 1(a). Each peanut consists of a spherical hydrophobic lobe of radius R_0 fused with a spherical hydrophilic lobe of radius R_1 . The centers of the two lobes are separated by a distance δ , which we quantify in dimensionless form via the parameter $\epsilon \equiv \delta/(R_0 + R_1)$. We fixed R_0 throughout (we consider R_0 to be approximately 50 nm), and investigated the behavior of the model as we varied ϵ and R_1/R_0 . We required $|R_1 - R_0|/(R_1 + R_0) < \epsilon \leq 1$; the lower inequality stipulates that one lobe may not be completely buried in the other, while the upper inequality requires lobes to be in contact. We define the orientation vector \mathbf{S}_i of peanut i to be the unit vector whose origin is the center of the hydrophobic lobe and which points diametrically away from the center of the hydrophilic lobe. Neighboring peanuts interact via hard-core excluded volume interactions – nothing may approach closer than R_0 (resp. R_1) to the center of each hydrophobic (resp. hydrophilic) lobe – and via a short-ranged, pairwise interaction modeling the attraction between solvated nanoscale hydrophobes [34] (we do not consider solvent explicitly in our model). We assume the hydrophobic interaction to be attenuated on a scale of approximately 5 nm, and impose an attractive interaction between the hydrophobic lobes of peanuts i and j of the form

$$U_{ij} = \epsilon_b \Theta(r_c - r_{ij}) A(\theta_{ij}) A(\theta_{ji}) (\mathcal{L}_\alpha(\hat{r}_{ij}) - \mathcal{L}_\alpha(\hat{r}_c)). \quad (1)$$

Here ϵ_b is a binding energy; $\hat{x} \equiv x/R_0 - 1$ is a shifted and scaled distance; r_{ij} is the distance between the centers of the hydrophobic lobes of i and j , respectively C_i and C_j ; $r_c \equiv 2.5R_0$ is a cutoff length; and $\mathcal{L}_\alpha(x) \equiv 4(x^{-2\alpha} - x^{-\alpha})$ is a generalized Lennard-Jones function. We take $\alpha = 15$ to ensure an attraction of sufficiently short range. In simulations we varied the attractive binding energy ϵ_b between limits of $4k_B T$ and $8k_B T$: corresponding forms of the radial component of the hydrophobic interaction potential are plotted in Figure 1(a). In experiment, variation of the strength of the hydrophobic driving force may be achieved by variation of temperature or solvent composition.

The factors A in Equation (1) parameterize an angular modulation of the attractive interaction, with θ_{ij} being the angle between \mathbf{S}_i and the vector pointing from C_i to C_j . This modulation enforces the tendency of two hydrophobes of girth exceeding 1 nm to maximize their surface-to-surface contact [34]. Its form is given and derived in the Appendix.

We performed simulations of collections of peanuts of given geometry, defined by their values of R_1/R_0 and ϵ , and for a range of values of the hydrophobic attraction strength ϵ_b . We used 1000 peanuts in a periodically-replicated cubic simulation box of side $64R_0$, corresponding to fixed mole fraction of colloid. The bulkiest ($R_1/R_0 = 2, \epsilon = 1$) and most compact ($R_1/R_0 = 0.2, \epsilon = 0.8$) peanuts we considered occupied volume fractions of about 14% and 1.5%, respectively (see Appendix). Starting from configurations in which peanuts were randomly mixed and oriented, we evolved each system according to the version of the virtual-move Monte Carlo algorithm [35] described in the Appendix of Ref. [36]. This algorithm is designed to mimic overdamped dynamics by making collective moves of particles according to the potential energy gradients, or forces, they experience; such collective moves are neglected by standard single-particle Monte Carlo algorithms. In brief, one particle is selected and subjected to a translation or a rotation. If changes in pairwise potential energies between that particle and its neighbors are favorable then the chosen particle moves independently; if not, neighbors are recruited iteratively and experience a collective displacement or translation. The acceptance rate for each move is chosen to preserve detailed balance and to reflect, in an approximate fashion, the (short-ranged) hydrodynamic drag suffered by the collective body. We scaled collective translation acceptance rates by the reciprocal of the approximate hydrodynamic radius of the moving body [35], and scaled acceptance rates for rotations by the cube of the same factor. Control of aggregate diffusion constant scalings provides one advantage of this method over conventional integration of overdamped equations of motion. We drew translation magnitudes from a uniform distribution with maximum $0.3R_0$, and drew rotation angles from a uniform distribution with maximum 13.6° (rotations were performed about a randomly-chosen axis through the midpoint of the line joining the centers of hydrophobic and hydrophilic lobes). This ability to make large trial translations and rotations of individual particles in the face of attractions and repulsions that vary rapidly with distance and angle is not shared by straightforward numerical integration schemes. Based on the diffusivity in water of a body of radius 50 nm, we estimate that our basic simulation timestep (an average of one attempted virtual move per particle) corresponds to $\sim 10^{-6}$ s. Our longest simulations exceeded 10^7 timesteps, implying that we probe ‘real’ timescales in excess of a second.

Our results are summarized by the ‘kinetic phase diagram’ of Figure 1(b). This diagram identifies those self-assembled products, whether equilibrated or kinetically trapped, accessible to dynamical simulation starting from well-mixed initial conditions. We expect by extension that such products will be accessible to experiments starting from similar conditions. The horizontal and vertical axes of this diagram label the quantities R_1/R_0 and ϵ , respectively; peanuts with small (resp. large) hydrophilic lobes are found to the left (resp. right) of the diagram. We identify regions of compact clusters (squares; see Fig 1(c)), non-spherical micelles (triangles), spherical micelles (circles; see Fig 1(f)) and bilayers (crosses; see Fig 1(d,e)). Our classification scheme and a summary of the computational resources we deployed are discussed in the Appendix. We find these phases to be localized in peanut

shape space largely in accord with a simple estimate of peanuts' molecular packing parameter [37, 38] (see Appendix): we have labeled the diagram with lines of packing parameter equal to 1 (the regime in which one expects bilayers); $1/2$ (the cylindrical micelle regime); and $1/3$ (the spherical micelle regime).

The phase most interesting from the materials scientist's perspective is perhaps the bilayer, because extended two-dimensional structures that do not require templating by a substrate are attractive candidates for device fabrication. Our observation that amphiphilic nanoscale peanuts can form bilayers, and that bilayer formation is localized to a specific region of peanut shape space, will facilitate the experimental search for this phase. We also observed bilayers to coexist with faceted hollow capsids composed of peanuts arranged with local bilayer-like order (see Fig 1(d)). We do not know why these structures coexist: they may represent comparable minima of free energy, or one may embody a particularly stable kinetic trap. This question will be the focus of future work. This observation nonetheless suggests that experimental realizations of this system can achieve multipotent self-assembly, wherein components may form coexisting, ordered phases of strikingly different symmetry. Some protein complexes appear to achieve such multipotent assembly by executing conformational changes [39].

Of the other phases observed, micelles are found abundantly for many peanut shapes, especially when the thermodynamic driving force for association is large and the formation of ordered structures like bilayers is hindered by kinetic traps. Micelle polydispersity may be controlled by varying R_1/R_0 (Fig. 2), suggesting a route to the synthesis of size-controlled nanometer scale assemblies. In addition, cluster formation is possible when the hydrophilic lobe is very small. Peanuts whose shapes lie on the left branch of the line $\epsilon = |R_1 - R_0|/(R_1 + R_0)$ in Figure 1(b) are isotropically attractive spheres, and form close-packed, crystalline clusters. Peanuts with very small hydrophilic lobes also form aggregates whose innermost particles make 12 pairwise contacts, although extended crystalline order is prevented by the anisotropic shape of the peanut.

While considerations of packing predict the phases we have found, with the exception of capsids, they give little insight into the complex dynamics of assembly we have observed. We found bilayer formation dynamics to be hierarchical (see Fig 3(a)), proceeding in a manner related to the two-step crystallization mechanism familiar from models of isotropically attractive particles [40, 41, 42, 43]. We focus on the dynamics associated with peanut state $(R_1/R_0, \epsilon_b) = (0.8, 0.2, 5k_B T)$. First, fluctional micelles appear. These can rearrange in a collective fashion to form a flattish, metastable proto-bilayer composed of about 7 close-packed peanuts per face, plus attendant edge particles (see Fig 3(a), left, circled). Such nuclei do not grow immediately, but do so only after an additional collective rearrangement that sees an abrupt increase in the number of bilayer-like particles comprising their core (see Fig 4(a,b)). As the nucleus exceeds a critical size of about 50 particles (Fig 4(b,c)), bilayer growth proceeds readily; the largest bilayers we observed exceeded 700 particles in size (Fig 4(f)). The time of the appearance of the first bilayer-like nucleus exceeding 50

particles in size is long and drawn from a broad distribution (from 30 independent simulations of $\sim 2.5 \times 10^7$ timesteps we observed the appearance of such structures in 14 cases; of this set, mean nucleation time was 1.6×10^7 timesteps – corresponding roughly to a rate of $10^{15} \text{ m}^{-3} \text{ s}^{-1}$ – with a standard deviation of 8×10^6 timesteps; see also Fig 4(d)). We have not explored in detail the dynamics of bilayer formation at other points in peanut shape space, but we present one example in Fig 3(b). Here a bilayer and a micelle merge before the former consumes the latter (see also Fig 4(d)).

Finally, we note that crystalline cluster formation by ‘peanuts’ whose hydrophilic lobes are of vanishing size proceeds via conventional two-step crystallization [40, 41, 42, 43]: first, dense liquid droplets nucleate from vapor; second, crystalline order nucleates within liquid droplets (not shown). It would make for an interesting theoretical study to determine the dynamics of assembly one proceeds into the regime of increasing hydrophilic lobe size: what is the nature of cluster formation as the crystal structure becomes suppressed or thermodynamically disfavored with respect to the dense liquid phase? Clusters in our simulations generally coalesce upon contact, suggesting that in experiment such assemblies would not be soluble, and would not be of great practical interest.

We have demonstrated that dynamical simulation of a simple model of nanoscale amphiphilic peanut-shaped colloids generates phases of clusters, micelles and bilayers in accord with expectations based on simple ideas of packing. We have also found certain ordered structures and observed complex dynamical mechanisms that cannot be so explained. We expect this model and its behavior to be prototypical of a class of amphiphilic structures now being synthesized in large quantities, and therefore to help guide the experimental search for new, functional nanostructured materials. Future theoretical work involving this model will focus on further quantifying the dynamical pathways observed in this study; determining the effect upon assembly of liquid-liquid interfaces [44]; and studying the design potential of multi-lobed peanut generalizations.

Note added in proof. As we finalized our manuscript a study by Miller and Cacciuto [33] appeared on the ArXiv. In this study the authors explored the self-assembly of spherical amphiphilic particles using molecular dynamics simulation. Interestingly, despite the differences in interaction range and particle shape between their model and ours, those authors also observed the coexistence of bilayers and hollow, faceted capsids. This implies that such coexistence is not dependent upon fine details of particle-particle interactions, but can be understood on more general grounds.

ACKNOWLEDGEMENTS

Work at the Molecular Foundry was supported by the U.S. Department of Energy under Contract No. DE-AC02-05CH11231. We thank Sander Pronk for a critical reading of the manuscript, and Andrea Pasqua, Lutz Maibaum and Phillip Geissler for useful discussions.

-
- [1] J. Tien, T. Breen, and G. Whitesides, *Journal of the American Chemical Society* **120**, 12670 (1998).
- [2] C. Mao, V. Thalladi, D. Wolfe, S. Whitesides, and G. Whitesides, *J. Am. Chem. Soc* **124**, 14508 (2002).
- [3] T. Breen, J. Tien, S. Oliver, T. Hadzic, and G. Whitesides, *Science* **284**, 948 (1999).
- [4] G. Whitesides and M. Boncheva, *PNAS* **99**, 4769 (2002).
- [5] G. Whitesides and B. Grzybowski, *Science* **295**, 2418 (2002).
- [6] E. Rabani, D. Reichman, P. Geissler, and L. Brus, *Nature* **426**, 271 (2003).
- [7] A. Boal, F. Ilhan, J. DeRouchey, T. Thurn-Albrecht, T. Russell, and V. Rotello, *Nature* **404**, 746 (2000).
- [8] C. Dobson, *Nature* **426**, 884 (2003).
- [9] H. Fraenkel-Conrat and R. Williams, *Proceedings of the National Academy of Sciences of the United States of America* **41**, 690 (1955).
- [10] J. Huie, *Smart Materials and Structures* **12**, 264 (2003).
- [11] S. Zhang, *Nature Biotechnology* **21**, 1171 (2003).
- [12] L. Maibaum, A. Dinner, and D. Chandler, *Journal of Physical Chemistry B* **108**, 6778 (2004).
- [13] U. Schwarz and G. Gompper, *Lecture Notes in Physics* pp. 107–151 (2002).
- [14] T. Landh, *FEBS letters* **369**, 13 (1995).
- [15] E. Mock, H. De Bruyn, B. Hawkett, R. Gilbert, and C. Zukoski, *Langmuir* **22**, 4037 (2006).
- [16] H. Sheu, M. El-Aasser, and J. Vanderhoff, *Journal of Polymer Science Part A: Polymer Chemistry* **28** (1990).
- [17] S. Bon et al., unpublished (2009).
- [18] A. Walther and A. Müller, *Soft Matter* **4**, 663 (2008).
- [19] P. Johnson, C. van Kats, and A. van Blaaderen, *Langmuir* **21**, 11510 (2005).
- [20] J. Kim, R. Larsen, and D. Weitz, *Adv. Mater* **16**, 274 (2004).
- [21] B. Huisman, P. Bolhuis, and A. Fasolino, *Phys. Rev. Lett* **100**, 188301 (2007).
- [22] M. Horsch, Z. Zhang, and S. Glotzer, *Physical Review Letters* **95**, 56105 (2005).
- [23] Z. Zhang, M. Horsch, M. Lamm, and S. Glotzer, *Nano Letters* **3**, 1341 (2003).
- [24] A. Wilber, J. Doye, A. Louis, E. Noya, M. Miller, and P. Wong, *The Journal of Chemical Physics* **127**, 085106 (2007).
- [25] Z. Zhang, A. Keys, T. Chen, and S. Glotzer, *Langmuir* **21**, 11547 (2005).
- [26] M. Hagan and D. Chandler, *Biophysical Journal* **91**, 42 (2006).
- [27] G. Villar, A. Wilber, A. Williamson, P. Thiara, J. Doye, A. Louis, M. Jochum, A. Lewis, and E. Levy, *Physical Review Letters* **102** (2009).
- [28] T. Ouldridge, I. Johnston, A. Louis, and J. Doye, *The Journal of Chemical Physics* **130**, 065101 (2009).

- [29] T. Chen, Z. Zhang, and S. Glotzer, *Proceedings of the National Academy of Sciences* **104**, 717 (2007).
- [30] L. Hong, A. Cacciuto, E. Luijten, and S. Granick, *Langmuir* **24**, 621 (2008).
- [31] O. Elrad and M. Hagan, *Nano Letters* **8**, 3850 (2008).
- [32] C. Iacovella and S. Glotzer, *Nano Letters* **9**, 1206 (2009).
- [33] W. Miller and A. Cacciuto, Arxiv preprint arXiv:0905.4236 (2009).
- [34] D. Chandler, *Nature* **437**, 640 (2005).
- [35] S. Whitelam and P. Geissler, *The Journal of Chemical Physics* **127**, 154101 (2007).
- [36] S. Whitelam, E. Feng, M. Hagan, and P. Geissler, *Soft Matter* **5**, 1251 (2009).
- [37] J. Israelachvili, D. Mitchell, and B. Ninham, *Journal of the Chemical Society, Faraday Transactions 2* **72**, 1525 (1976).
- [38] R. Nagarajan, *Langmuir* **18**, 31 (2002).
- [39] S. Whitelam, C. Rogers, A. Pasqua, C. Paavola, J. Trent, and P. Geissler, *Nano Letters* (2008).
- [40] P. Wolde and D. Frenkel, *Science* **277**, 1975 (1997).
- [41] B. Chen, H. Kim, S. Keasler, and R. Nellas, *J. Phys. Chem. B* **112**, 4067 (2008).
- [42] J. van Meel, A. Page, R. Sear, and D. Frenkel, *The Journal of Chemical Physics* **129**, 204505 (2008).
- [43] A. Fortini, E. Sanz, and M. Dijkstra, *Physical Review E* **78** (2008).
- [44] D. Cheung and S. Bon, *Physical Review Letters* **102**, 066103 (2009).
- [45] D. Frenkel and B. Smit, *Understanding Molecular Simulation: From Algorithms to Applications* (Academic Press, 2002).
- [46] W. Humphrey, A. Dalke, and K. Schulten, *Journal of Molecular Graphics* **14**, 33 (1996).

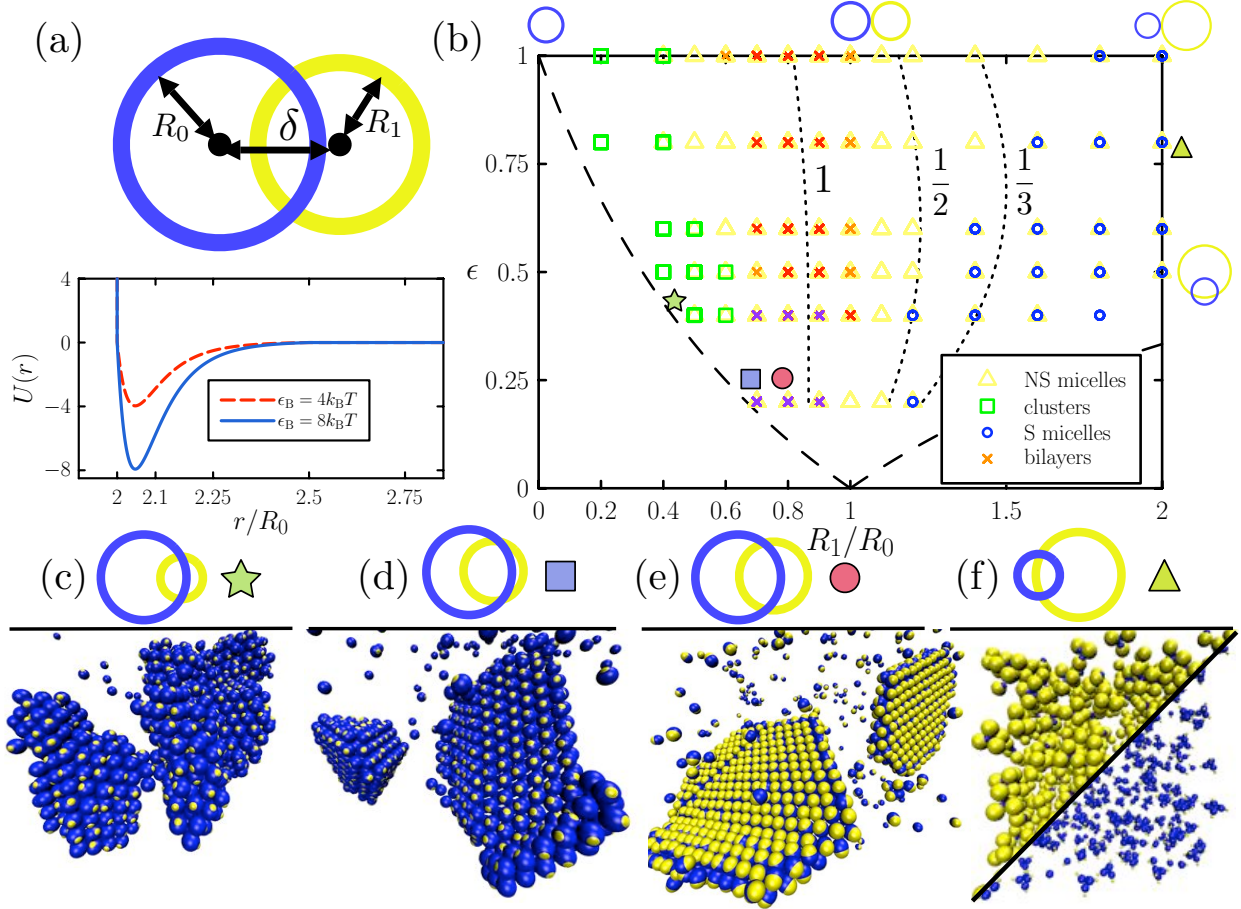


FIG. 1: Model geometry and kinetic phase diagram identifying products of self-assembly. (a) Peanut geometry with hydrophobic (resp. hydrophilic) lobe shown in blue (resp. yellow), together with the radial component of the blue-blue interaction potential. (b) Kinetic phase diagram in the space of $\epsilon \equiv \delta/(R_0 + R_1)$ and R_1/R_0 identifying the products found following dynamic simulations of peanuts with specified geometries (see text for classification of bilayers, micelles and clusters). Examples of such products: (c) coalesced compact clusters at thermodynamic state $(R_1/R_0, \epsilon, \epsilon_b) = (0.5, 0.4, 4.5k_B T)$; (d) coexisting bilayer and hollow faceted capsid at $(R_1/R_0, \epsilon, \epsilon_b) = (0.7, 0.2, 5k_B T)$; (e) bilayers at state $(R_1/R_0, \epsilon, \epsilon_b) = (0.8, 0.2, 5k_B T)$; and (f) spherical micelles at $(R_1/R_0, \epsilon, \epsilon_b) = (2, 0.8, 8k_B T)$ (bottom right shows hydrophilic lobes reduced in size for clarity). Contours of constant packing parameter (values indicated) are dotted lines; the dashed lines indicate the two branches satisfying $\epsilon = |R_1 - R_0|/(R_1 + R_0)$. Below these lines one lobe of the ‘peanut’ is completely buried within the other.

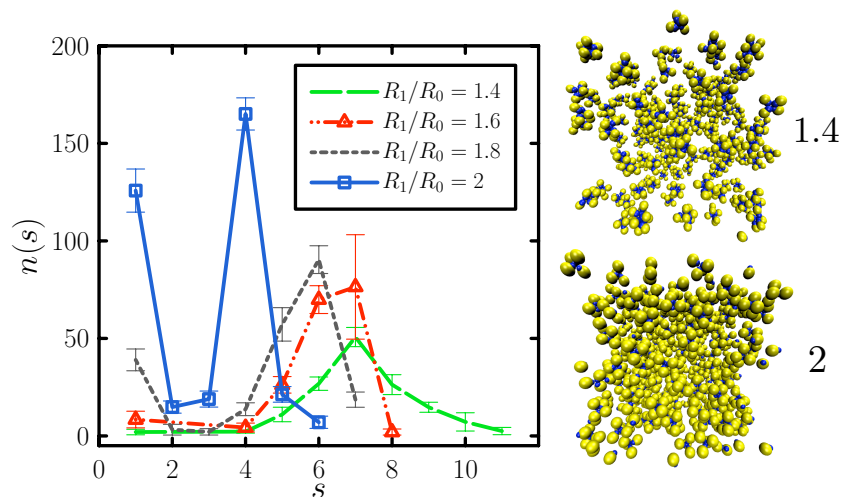


FIG. 2: Micelle polydispersity. Number of aggregates of size s , $n(s)$, for micelle-forming peanuts satisfying $\epsilon = 1/2$ and $\epsilon_b = 8k_B T$. Varying R_1/R_0 , which is achievable synthetically, controls micelle polydispersity. Each line was obtained using 10 independent simulations evolved for $\sim 5 \times 10^6$ timesteps.

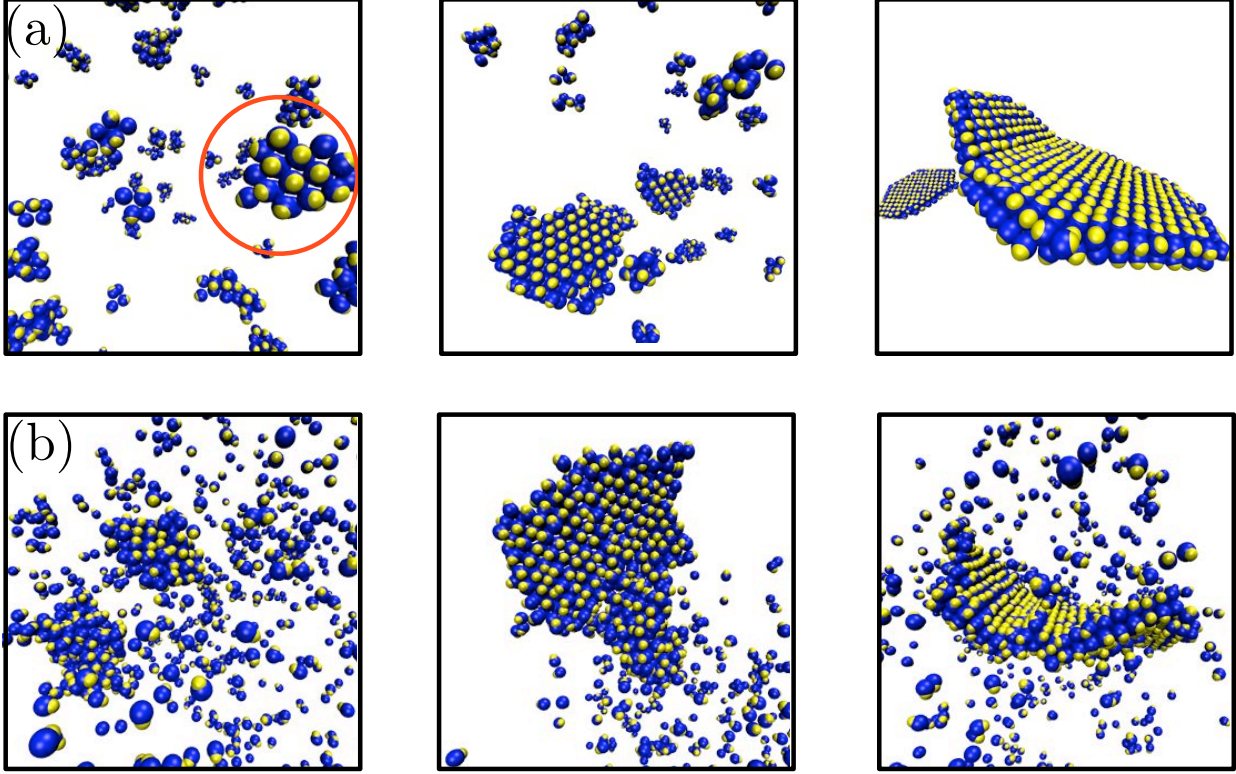


FIG. 3: Time-ordered configurations demonstrating two different hierarchical self-assembly pathways. (a) Example from thermodynamic state $(R_1/R_0, \epsilon, \epsilon_b) = (0.8, 0.2, 5k_B T)$: One of several micelles formed at early times eventually undergoes a collective internal rearrangement and attains a metastable proto-bilayer configuration (left, circled, $t \approx 1.1 \times 10^7$). When this aggregate exceeds a critical size it grows readily, with particles on its perimeter collectively rearranging to allow the attachment of more material. It is later joined by a second bilayer (center, $t \approx 1.4 \times 10^7$). These two bilayers grow until together they possess about 800 of the 1000 peanuts in the simulation box (right, $t \approx 2.7 \times 10^7$). Only aggregates of size >3 are shown. (b) Example from state $(R_1/R_0, \epsilon, \epsilon_b) = (0.7, 0.4, 4.5k_B T)$: a bilayer and a micelle grow (left, $t \approx 4.5 \times 10^6$) and merge (center, $t \approx 8.5 \times 10^6$). The bilayer eventually absorbs the micelle and continues to grow (right $t \approx 1.2 \times 10^7$).

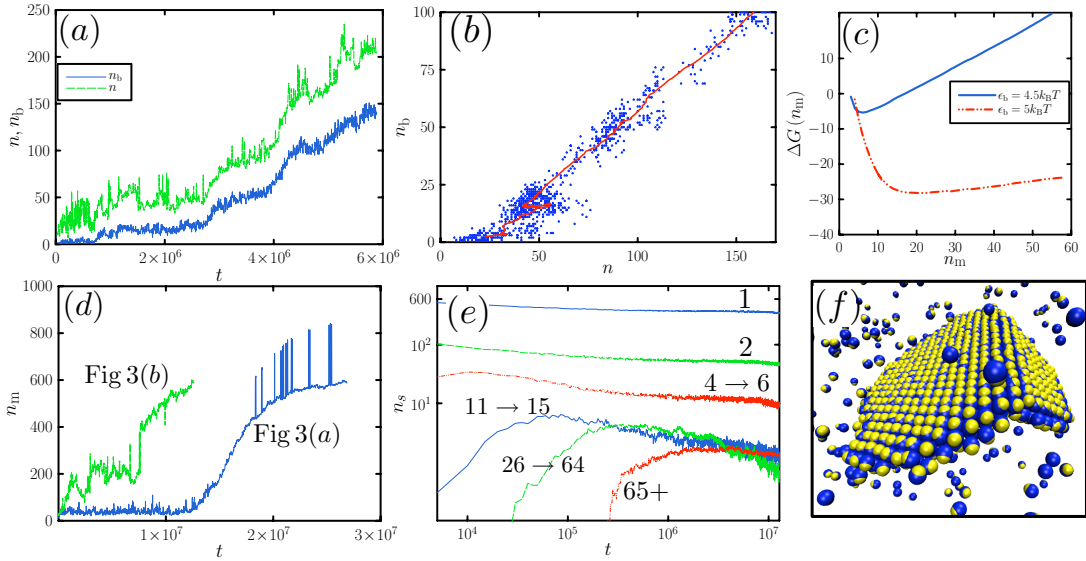


FIG. 4: Measurements of bilayer self-assembly. (a) Number of particles n and number of bilayer-like particles n_b (see Appendix) comprising an aggregate found at the thermodynamic conditions used to generate Fig 3(a), namely $(R_1/R_0, \epsilon, \epsilon_b) = (0.8, 0.2, 5k_B T)$. The establishment of a sufficiently large bilayer-like core, which occurs in stages, is necessary for large-scale growth. These quantities are plotted parametrically in (b), with running average shown in red. (c) Free energy as a function of largest aggregate size, n_m , at the same thermodynamic state, together with the corresponding curve at $\epsilon_b = 4.5k_B T$. We used standard umbrella sampling [45]. Small micelles are favored at the smaller binding energy. At the larger binding energy there is a thermodynamic driving force to condense a micelle, with a broad valley separating micelle from bilayer. While no large barrier separates these two morphologies, dynamical simulation suggests the rate at which this valley is explored is slow. Future work will focus on exploring this free energy landscape in a space of n and n_b . (d) Size of largest aggregate n_m versus time for the systems depicted in Fig 3(a) and -(b). Curve ‘Fig3(a)’ shows the long time proceeding bilayer formation, as well as occasional collisions between the two bilayers that form; curve ‘Fig3(b)’ records the micelle-bilayer collision and the subsequent growth of the bilayer. (e) Number of aggregates of specified sizes versus time for a 1000-peanut system, averaged over 30 independent simulations, at state $(R_1/R_0, \epsilon, \epsilon_b) = (0.8, 0.2, 5k_B T)$. This plot reveals the considerable time required for the construction of large aggregates. (f) Bilayer comprising about 740 peanuts found at the same thermodynamic state. Its faceting foreshadows that seen in capsids at thermodynamic state $(R_1/R_0, \epsilon, \epsilon_b) = (0.7, 0.2, 5k_B T)$.

APPENDIX

Angular modulation of the hydrophobic interaction. The factors A in Equation (1) have the following origin (refer to Figure 5 for geometry). We assume the strength of the hydrophobic attraction on the lengthscales we consider to be proportional to the contacting surface area between two hydrophobic bodies [34]. We define two surfaces to be ‘in contact’ if they lie no further than 5 nm apart, reflecting our assessment of the likely range of the hydrophobic force. If two spheres of radius $R_0 \approx 50$ nm are placed in contact, the plane half-angle subtended by the limit of the ‘contacting’ surface area at the center of either sphere is $\psi \equiv \arccos(1-5/(2 \cdot 50)) \approx 18.1^\circ$ (peanuts are azimuthally symmetric about their orientation vector, and so we consider only plane angles, as sketched in Figure 5). Hence we argue that the hydrophobic lobe of peanut i presents its maximum possible surface area to a similar body B if the angle between \mathbf{S}_i and the vector pointing from C_i to the center of B is *not* within an angle ψ of the line joining C_i to the nearest surface obstruction.

We next define the angle θ_{\max} to be the angle between \mathbf{S}_i and the line joining C_i to the largest obstruction provided by each hydrophobic lobe’s hydrophilic partner. This angle is given by geometrical considerations. The angle between \mathbf{S}_i and the line joining C_i to the intersection of hydrophobic and hydrophilic lobes is $\theta_{\text{intersec}} = \pi - \arccos(\ell/R_0)$, where $\ell \equiv \delta/2 - (R_1^2 - R_0^2)/(2\delta)$ (note that ℓ may be negative). The angle between \mathbf{S}_i and the line joining C_i to the greatest diameter presented by its hydrophilic partner is $\theta_{\text{girth}} = \pi - \arctan(R_1/\delta)$. We take $\theta_{\max} = \min(\theta_{\text{intersec}}, \theta_{\text{girth}})$. In Figure 1 (a) we see that $\theta_{\max} = \theta_{\text{intersec}}$ for the particular peanut geometry sketched there.

To construct the function $A(\theta)$ we argue as follows. Let θ be the angle between \mathbf{S}_i and the line joining C_i to the center of a similar body B. For $\theta = 0$ the peanut i presents its maximum possible hydrophobic surface area to B. Conversely, the greatest obstruction of the hydrophobic lobe caused by the hydrophilic lobe occurs when $\theta = \pi$, i.e. when the body B approaches the peanut from its hydrophilic side. This obstruction can be total, if the hydrophilic lobe is sufficiently large, or less than total, if the hydrophilic lobe is small and/or well-buried within its hydrophobic partner. We take the smallest possible ‘signal’ presented by the hydrophobic surface of peanut i to the body B to be $A_{\min} = \max(0, 1 - (\pi - \theta_{\max})/\psi)$. Finally, we assume for simplicity that the signal interpolates linearly with θ between its largest and smallest values, i.e $A(\theta) \propto -\theta$ if B lies in the penumbra cast by the hydrophilic lobe, i.e. when θ exceeds $\theta_{\max} - \psi$. These arguments imply the following piecewise linear form for the angular modulation function in Equation (1):

$$A(\theta) = \begin{cases} 1 & (\theta < \phi) \\ \max(A_{\min}, 1 - \frac{1}{2\psi}(\theta - \phi)) & (\theta \geq \phi), \end{cases} \quad (2)$$

where $\phi \equiv \theta_{\max} - \psi$. In Figure 5 we plot $A(\theta)$ for two peanut geometries. We note that for the nanoscale particles we have studied here, identification of the length and angular scales over which the hydrophobic effect operates reveals that multibody forces between particles

are neither required nor warranted.

Peanut volume. The volume presented to solvent by two fused spheres of radii R_0 and R_1 whose centers are δ apart ($|R_1 - R_0| < \delta \leq (R_1 + R_0)$) is given from geometrical considerations by

$$\begin{aligned} V_{\text{peanut}} &= \frac{4}{3}\pi(R_0^3 + R_1^3) - \pi \int_{\ell}^{R_0} dx(R_0^2 - x^2) \\ &\quad - \pi \int_{\delta-\ell}^{R_1} dx(R_1^2 - x^2) \\ &= \frac{(1 + \epsilon)^2}{12\epsilon} \pi \Sigma (3\Delta^2 + \epsilon(2 - \epsilon)\Sigma^2). \end{aligned} \quad (3)$$

Here $\epsilon \equiv \delta/(R_0 + R_1)$, $\ell \equiv \delta/2 - (R_1^2 - R_0^2)/(2\delta)$, $\Sigma \equiv R_0 + R_1$ and $\Delta \equiv R_0 - R_1$. This formula may be used to calculate the fraction of the simulation box occupied by peanuts of arbitrary geometry.

Computational details. To obtain Figure 1(b) we performed simulations for times sufficient to observe what we believe to be steady-state behavior at each location in peanut shape space. In the regime $R_1/R_0 \geq 1.2$ (the micelle-forming regime) this is straightforward: for each point in the $(R_1/R_0, \epsilon)$ plane we performed one simulation at each of $\epsilon_b = (5, 6, 7, 8)k_B T$ for $\sim 5 \times 10^6$ timesteps (60 CPU hours per simulation). In the cluster-forming regime of $R_1/R_0 \leq 0.4$ we performed 5 independent simulations at each labeled point for each value of $\epsilon_b = (4, 4.5, 5, 5.5)k_B T$, also for $\sim 5 \times 10^6$ timesteps each (60 CPU hours per simulation). In the intermediate regime $0.4 < R_1/R_0 < 1.2$ we found some bilayers to form only after very long times. We therefore performed 5 independent simulations of $\sim 5 \times 10^6$ timesteps each (60 CPU hours per simulation) at each point for each value of $\epsilon_b = (4, 4.5, 5, 5.5)k_B T$, and in addition performed three further independent simulations of $\sim 2.5 \times 10^7$ timesteps (300 CPU hours per simulation) at each point for each of the four values of ϵ_b . Along the line $R_1/R_0 = 1$ we performed three additional simulations of $\sim 2.5 \times 10^7$ timesteps for each value of $\epsilon_b = (6, 6.5)k_B T$. We can of course not rule out the likelihood of nucleation and growth of structures on timescales longer than those we probed, nor rule out the appearance of other interesting ordered structures at values of ϵ_b that we did not consider. To obtain Figure 2 we performed 10 additional simulations of $\sim 5 \times 10^6$ timesteps at each of the four thermodynamic states shown (60 CPU hours per simulation). To obtain Figure 4 we performed 30 additional independent simulations of $\sim 2.5 \times 10^7$ timesteps (300 CPU hours per simulation) at thermodynamic state $(R_1/R_0, \epsilon, \epsilon_b) = (0.8, 0.2, 5k_B T)$.

Classification of self-assembled structures. We classified the products of peanut self-assembly by analyzing the final configuration of each simulation as follows. We define contacting peanuts to be those possessing a pairwise energy of interaction of $-k_B T$ or less. We define

an ‘aggregate’ to be a contiguous set of contacting particles. We identified locations in peanut shape space to contain ‘clusters’ (compact structures with some degree of close packing) if any particle possessed 12 contacts. We identified micelles by calculating for each aggregate the number $\mathcal{M} \equiv N_a^{-1} \sum_{i=1}^{N_a} \mathbf{S}_i \cdot (\mathbf{r}_{\text{CM}} - \mathbf{r}_i)$. Here N_a is the number of peanuts comprising the aggregate, \mathbf{r}_{CM} is the center of mass of the aggregate, and \mathbf{r}_i is the position of aggregate constituent i (all coordinates are corrected for periodic boundaries). If any location in shape space contained at least three aggregates of size three or greater that scored $\mathcal{M} \geq 0.9$ then we considered that state to contain spherical micelles, and marked that state with a circle. Any location with three or more aggregates of size three scoring $0.5 \leq \mathcal{M} < 0.9$ is considered to contain nonspherical micelles, and was marked with a triangle. Bilayer order was identified on the basis of the order parameter $\mathcal{B} \equiv 2(N_a(N_a - 1))^{-1} \sum_{(ij)} (\mathbf{S}_i \cdot \mathbf{S}_j)^2$, where the sum runs over all particle pairs in the aggregate ($\mathcal{B} = \frac{1}{3}$ for collections of randomly-oriented peanuts). Configurations possessing an aggregate of (25,50,200) constituents or more having a score of $\mathcal{B} \geq 0.4$ were marked with an (orange, red, purple) cross. In Figure 4 we show for one aggregate the number of its constituents possessing local bilayer-like order, n_b . To compute this quantity we formed the dot product of the orientation vector of a given particle and each of its neighbors’ orientation vectors. We define a ‘bilayer-like’ particle as one possessing 3 or more neighbors with which it has orientation-orientation dot product > 0.8 , and 1 or more neighbors with which it has dot product < -0.8 . This order parameter is not useful for examining clusters, whose internal particles associate in an orientationally disordered way and can test ‘false positive’ for local bilayer ordering. However, it does successfully distinguish between regions of local order and disorder in the bilayer-forming regime of peanut shape space. For most conditions considered it is possible to find amorphous structures answering to none of the above descriptions. This is most often true when the hydrophobic driving force is very strong, and kinetically frustrated aggregates form. We have ignored these structures, focusing on the ordered products we have described. While the order parameters and the threshold numbers we have applied are arbitrary, and the extent of each regime varies as the structural classification criteria are varied, we consider the trends we have identified to be representative of the nature of the self assembly we observed. Some additional structures are shown in Fig 6. We used VMD [46] to render simulation configurations in this paper.

Packing parameter. Considerations of packing have been used with success to predict the phases formed by molecular surfactants [37, 38]. We can define a packing parameter for an aggregate as $P_{\text{agg}} \equiv V_{\text{agg}}/(a_{\text{agg}}L_{\text{agg}})$, where V_{agg} is aggregate volume, a_{agg} its surface area, and L_{agg} a characteristic length. For a cylinder of radius R and length ℓ , for example, $V_{\text{cylinder}} = \pi R^2 \ell$, $L_{\text{cylinder}} = R$, and $a_{\text{cylinder}} = 2\pi R \ell$, giving $P_{\text{cylinder}} = 1/2$. Analogously, $P_{\text{sphere}} = 1/3$ and $P_{\text{bilayer}} = 1$. If we now assume such shapes to be composed of amphiphilic components, then, loosely, a_{agg} corresponds to the total area presented to solvent by hydrophilic groups, while V_{agg} and L_{agg} are the volumes and characteristic lengths of the hydrophobic units.

If one assumes that P_{agg} can be estimated from the geometry of a *single* amphiphile (see, however, Ref. [38]), then values of $P_{\text{single}} \equiv P$ near 1, 1/2 or 1/3 suggest self-assembly of bilayers, cylindrical micelles or spherical micelles, respectively. We can make a rough estimate of P for an individual peanut. If we assume that hydrophobic and hydrophilic lobes touch but do not interpenetrate, then $V = \frac{4}{3}\pi R_0^3$, $L = 2R_0$ and $a = \pi R_1^2$. We thus have $P = \frac{2}{3}(R_0/R_1)^2$. To this approximation, therefore, contours of constant P are vertical lines on Figure 1(b). Furthermore, $P = 1 \implies R_1/R_0 = \sqrt{2/3} \approx 0.82$ and $P = 1/3 \implies R_1/R_0 = \sqrt{2} \approx 1.41$. From Figure 1(b) we indeed find bilayers and spherical micelles in the corresponding regimes. A more refined estimate based on peanut geometry alone may be made by accounting for the volume of the hydrophobic lobe buried within the hydrophilic lobe. We have

$$V = \frac{4}{3}\pi R_0^3 - \pi \int_{\ell}^{R_0} dx(R_0^2 - x^2), \quad (4)$$

$L = R_0 + \ell$, and $a = \pi R_1^2$ (valid when the hydrophilic lobe's greatest diameter is not buried within the hydrophobic lobe; if this is *not* true, then $a = \pi(R_0^2 - \ell^2)$). Contours of $P = 1$, $P = 1/2$ and $P = 1/3$ to this approximation are plotted in Fig 1(b).

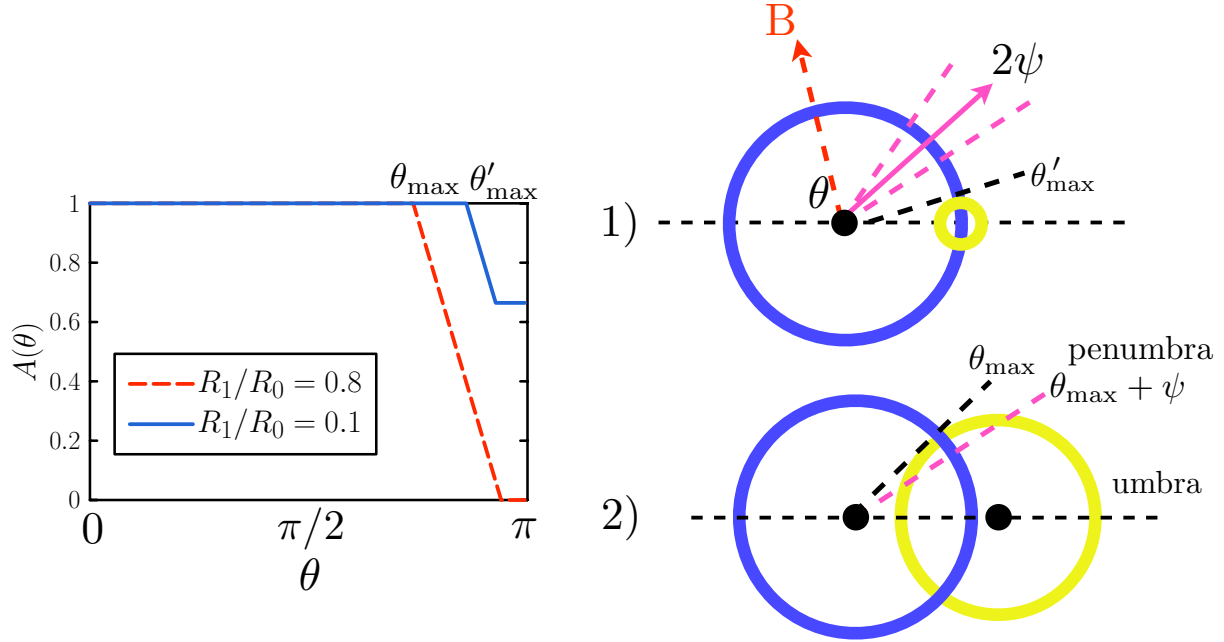


FIG. 5: Angular modulation function $A(\theta)$, designed to account for the degree of contact made by hydrophobic lobes of adjacent peanuts. θ is the plane angle between the peanut orientation vector and the vector pointing from the center of the hydrophobic lobe (blue) to the center of a similar body, B . We plot $A(\theta)$ for peanuts of geometry 1) $(R_1/R_0, \epsilon) = (0.1, 0.85)$ and 2) $(R_1/R_0, \epsilon) = (0.8, 0.85)$. ‘Penumbra’ and ‘umbra’ identify the regions for which, respectively, partial and total occlusion of the blue lobe is caused by the yellow lobe. See text for details.

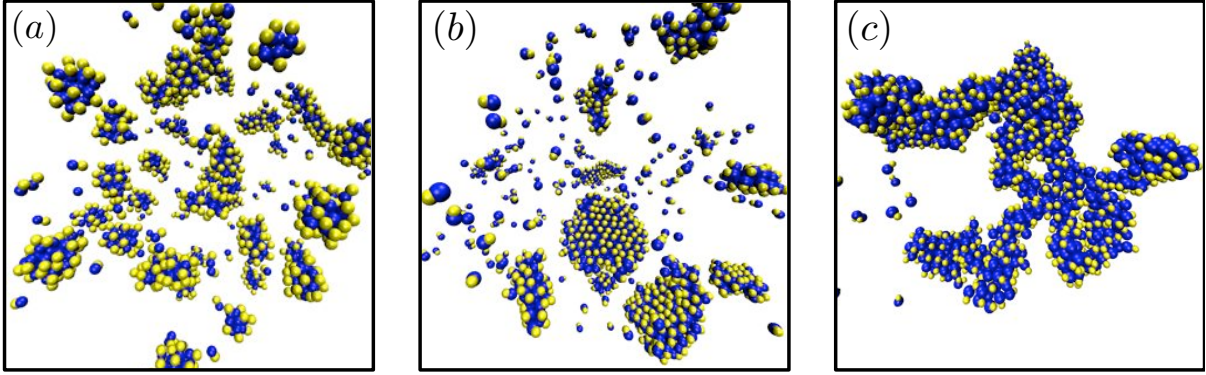


FIG. 6: Additional configurations. (a) Micelles of various morphologies found at thermodynamic state $(R_1/R_0, \epsilon, \epsilon_b) = (1, 0.8, 5.5k_B T)$; (b) Coexisting bilayers and micelles at state $(R_1/R_0, \epsilon, \epsilon_b) = (0.8, 0.5k_B T)$; and (c) disordered wormlike micelle at state $(R_1/R_0, \epsilon, \epsilon_b) = (0.6, 0.8, 5k_B T)$.